STM JOURNALS

Journal of
Polymer & Composites

https://journals.stmjournals.com/jopc

ISSN: 2321-2810 (Online)
ISSN: 2321-8525 (Print)
Volume 14, Special Issue 4, 2026
January–December
DOI (Journal): 10.37591/JoPC

Research JoPC

Fabrication, Interfacial Characterization, and Superparamagnetic Properties of Fe_3O_4@γ-Fe_2O_3 Core/Shell Nanoparticle-Reinforced Chitosan Biopolymer Composites

Rajeshwar Rai[1,*], Anup Kumar Mishra[2], Dhananjai Singh[3], Rajnish Kumar Singh[4]

Abstract

Magnetite/maghemite core/shell nanoparticles were prepared by alkaline co-precipitation of Fe(II) and Fe(III) precursors followed by controlled thermal oxidation at 350°C and subsequently incorporated into chitosan at 1, 3, and 5 wt% loadings by solution casting. The resulting films were evaluated by X-ray diffraction (XRD), Fourier-transform infrared spectroscopy (FT-IR), high-resolution transmission electron microscopy (HR-TEM), vibrating-sample magnetometry (VSM), thermogravimetric analysis (TGA), and tensile testing. XRD showed characteristic cubic spinel reflections at 2θ ≈ 30.15°, 35.48°, 43.12°, 53.45°, 57.02°, and 62.61°, with an apparent crystallite size of approximately 13.8 nm and a lattice parameter of 0.8362 nm. HR-TEM showed approximately spherical particles in the 12–16 nm range; contrast analysis gave a magnetite-rich inner region of about 9.5 nm and an oxidized outer region of about 2.2 nm, yielding an overall dimension consistent with the XRD-derived size. FT-IR bands shifted from approximately 3420 to 3385 cm^{-1} and from 1592 to 1585 cm^{-1} after filler incorporation, while an Fe–O vibration appeared near 582 cm^{-1}, supporting interfacial interaction between chitosan functional groups and the iron-oxide surface. At 300 K, the composite films displayed negligible remanence and coercivity under the reported measurement conditions, consistent with a highly reversible superparamagnetic-like response. The 5 wt% film exhibited the strongest combined property enhancement: tensile strength increased from 32.4 to 53.1 MPa (≈64%), Young's modulus from 1.15 to 2.38 GPa, and the reported TGA degradation onset from 225 to 258°C. These results support the use of low-loading Fe_3O_4@γ-Fe_2O_3/chitosan films as magnetically responsive, mechanically reinforced biopolymer composites for separation, adsorption, sensing, and related functional-material applications.

***Author for Correspondence**
Rajeshwar Rai
E-mail: rajeshwarrai@mitmuzaffarpur.org

[1]Assistant Professor, Department of Chemistry, MIT Muzaffarpur, Department of Science, Technology and Technical Education, Bihar Engineering University, Patna, Bihar, India
[2]Assistant Professor, Department of Chemistry, M.I.T Muzaffarpur, Technology and Technical Education, Bihar Engineering University, Patna, Bihar, India
[3]Assistant Professor, Department of Chemistry, Nalanda College of Engineering, Chandi, Nalanda, Bihar, India
[4]Lecturer, Department of Chemistry, Government Polytechnic Chapra, DSTTE, Bihar, India

Received Date: August 16, 2026
Accepted Date: September 08, 2026
Published Date: September 10, 2026

Citation: Rajeshwar Rai, Anup Kumar Mishra, Dhananjai Singh, Rajnish Kumar Singh. Fabrication, Interfacial Characterization, and Superparamagnetic Properties of Fe_3O_4@γ-Fe_2O_3 Core/Shell Nanoparticle-Reinforced Chitosan Biopolymer Composites. Journal of Polymer & Composites. 2026; 14(Special Issue 4): S932–S942p.

Keywords: Fe_3O_4@γ-Fe_2O_3, chitosan, core/shell nanoparticles, magnetic nanocomposites, interfacial interaction, superparamagnetic-like response, XRD, thermal stability

INTRODUCTION

Magnetic iron-oxide nanoparticles are widely investigated because their magnetic response, surface chemistry, redox activity, and nanometre-scale dimensions can be tailored for applications in separation, catalysis, sensing, imaging, and functional composite materials [1–4]. Magnetite (Fe_3O_4) is an inverse-spinel oxide containing Fe^{2+} and Fe^{3+} distributed between tetrahedral and octahedral sites. Electron exchange between Fe^{2+} and Fe^{3+} in octahedral sites contributes to its comparatively high room-temperature magnetization, while decreasing particle size can lead to single-domain behavior and thermally activated moment reversal [5–7].

© STM Journals 2026. All Rights Reserved

Magnetite is susceptible to oxidation. Conversion of Fe^{2+} to Fe^{3+} produces maghemite (γ-Fe_2O_3), which retains a defect-spinel framework but generally exhibits a lower saturation magnetization than stoichiometric magnetite. Controlled surface oxidation can, therefore, generate a magnetite-rich core surrounded by a maghemite-rich oxidized region. This architecture is attractive because the outer oxidized layer passivates the more reactive magnetite-rich interior while preserving substantial magnetic functionality. Dave and Kalaniya reported Fe_3O_4@γ-Fe_2O_3 core/shell nanoparticles produced by co-precipitation followed by thermal treatment, providing a direct precedent for low-temperature oxidation of magnetite nanoparticles [8].

A second challenge is nanoparticle aggregation. Bare magnetic nanoparticles have high specific surface energy and experience dipole–dipole interactions that promote clustering, which can reduce accessible surface area and compromise processability [9, 10]. Immobilizing the nanoparticles in a polymer matrix can reduce direct particle–particle contact, improve handling, and create mechanically continuous materials. Chitosan is particularly attractive because it is a film-forming polysaccharide containing abundant amino and hydroxyl groups. These groups participate in hydrogen bonding and can interact with iron-oxide surfaces, providing a chemically active interface between the inorganic and organic phases [11, 12].

Magnetic chitosan systems have been explored in several configurations. Wu et al. prepared Fe_3O_4-chitosan nanoparticles for enzyme immobilization [13], whereas Soares et al. examined the thermal and magnetic behavior of chitosan-iron oxide nanoparticles [14]. Glutaraldehyde-cross-linked magnetic chitosan materials have been evaluated for dye removal [15], and soft-solution synthesis has been used to generate chitosan/iron-oxide nanocomposites with useful magnetic properties [13]. Magnetic chitosan microparticles, nanocubes, and hybrid hydrogels have also been investigated for enzyme immobilization, adsorption, and magnetically responsive biomedical systems [16–19]. These studies establish chitosan as a versatile host but also show that particle size, surface oxidation state, filler fraction, and interfacial chemistry strongly influence final performance.

The present study examines low-loading Fe_3O_4@γ-Fe_2O_3/chitosan films prepared by solution casting and correlates structural, interfacial, magnetic, mechanical, and thermal characteristics across 1, 3, and 5 wt% filler levels. The central objective is not simply to demonstrate magnetic response, but to relate the reported spinel nanostructure and chitosan–iron–oxide interfacial interaction to the observed reinforcement and thermal stabilization. Particular care is taken to distinguish evidence that is consistent with a magnetite-rich core/maghemite-rich surface from measurements that would be required for phase-specific proof of the core/shell chemistry.

MATERIALS AND METHODS

Materials

Ferric chloride hexahydrate ($FeCl_3 \cdot 6H_2O$, 98%), ferrous chloride tetrahydrate ($FeCl_2 \cdot 4H_2O$, 99%), sodium hydroxide (NaOH, 98%), hydrochloric acid, and glacial acetic acid were used for nanoparticle synthesis and polymer processing. Low-molecular-weight chitosan with a degree of deacetylation of approximately 85% was used as the polymer matrix. Deionized water (18.2 MΩ·cm) was used for solution preparation and washing. Chemical sources were recorded as Sigma-Aldrich for the iron salts, NaOH, and acetic acid, and Merck for chitosan in the supplied experimental record.

Preparation of Fe_3O_4 Precursor Nanoparticles

Fe_3O_4 precursor nanoparticles were prepared by alkaline co-precipitation under nitrogen. $FeCl_3 \cdot 6H_2O$ (0.54 g, 2.0 mmol) and $FeCl_2 \cdot 4H_2O$ (0.26 g, approximately 1.3 mmol) were dissolved in 50 mL of deoxygenated 0.05 M HCl and stirred at approximately 500 rpm at 30°C. A 1.5 M NaOH solution was added dropwise until the pH reached approximately 11, producing an immediate black precipitate. Stirring was continued for 30 min. The solid was magnetically separated using a neodymium magnet, washed repeatedly with deionized water and absolute ethanol, and vacuum-dried at 100°C for 1 h. The idealized magnetite precipitation reaction is:

© STM Journals 2026. All Rights Reserved

$Fe^{2+} + 2Fe^{3+} + 8OH^- \rightarrow Fe_3O_4 + 4H_2O$

Controlled Surface Oxidation to Fe_3O_4@γ-Fe_2O_3

The dried magnetite precursor was heated in an open-air muffle furnace at 350°C for 2.5 h. The treatment produced a black-to-reddish-brown colour change and was used to generate an oxidized γ-Fe_2O_3-rich surface region around a magnetite-rich interior. Because magnetite and maghemite have closely related spinel diffraction patterns, the term Fe_3O_4@γ-Fe_2O_3 in this work denotes the intended magnetite-rich core/oxidized maghemite-rich shell architecture supported by the synthesis history and nanoscale contrast analysis rather than an XRD-only phase assignment.

Preparation of Chitosan Solution and Nanocomposite Films

Chitosan (1.0 g) was dissolved in 50 mL of 1% (v/v) aqueous acetic acid at 40°C under continuous stirring for 4 h to obtain a homogeneous 2 wt% solution. Fe_3O_4@γ-Fe_2O_3 nanoparticles were added at 1, 3, and 5 wt% relative to the dry chitosan mass (0.01, 0.03, and 0.05 g per 1.0 g chitosan, respectively). Each nanofiller portion was dispersed in 10 mL of deionized water and ultrasonicated for 30 min before gradual addition to the chitosan solution. The mixtures were subjected to high-shear mixing at approximately 1200 rpm for 2 h, degassed under vacuum, cast onto Teflon Petri dishes (nominal diameter 90 mm), and dried at 50°C for 24 h. The resulting films had a nominal thickness of approximately 60 μm and are denoted CS-0, CS-1, CS-3, and CS-5 for 0, 1, 3, and 5 wt% magnetic filler, respectively. The overall workflow is summarized in Figure 1.

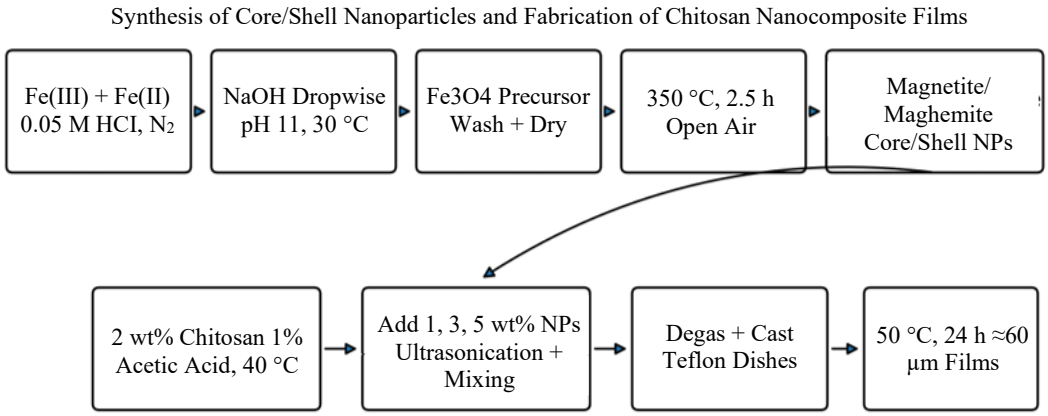


Figure 1. Schematic workflow for synthesis of the Fe_3O_4@γ-Fe_2O_3 magnetic nanofiller and solution-casting fabrication of chitosan nanocomposite films.

Structural, Spectroscopic, Microscopic, Thermal, Mechanical, and Magnetic Characterization

X-ray diffraction measurements were recorded on a Rigaku D/max 2500 VB/PC diffractometer using Cu-Kα radiation (λ = 0.15418 nm) at 40 kV and 40 mA over 2θ = 10–70°. Apparent crystallite size was calculated with the Scherrer relation [20], using K = 0.89 and the full width at half maximum in radians:

$$D = K\lambda / (\beta \cos \theta)$$

For a cubic lattice, the lattice parameter was obtained from indexed interplanar spacings using $a = d_{hkl}\sqrt{(h^2 + k^2 + l^2)}$. FT-IR spectra were recorded on a Nicolet FTIR 5SXC spectrometer over 4000-400 cm^{-1} at 4 cm^{-1} resolution using KBr-based sample preparation. HR-TEM was performed on a JEOL JEM-2100F field-emission transmission electron microscope at 200 kV. Magnetic measurements were obtained at 300 K on a Quantum Design PPMS/VSM system over applied fields up to ±15 kOe. TGA was performed on a TA Instruments Q50 under nitrogen (50 mL min^{-1}) from 30 to 700°C at 10°C min^{-1}. Tensile strength and Young's modulus were obtained using a universal mechanical testing system under a consistent test protocol for all film formulations.

© STM Journals 2026. All Rights Reserved

The supplied dataset contained reported property values but did not include replicate-level standard deviations or raw instrumental files. Accordingly, the numerical comparisons below are descriptive. Where a mechanistic interpretation depends on measurement normalization or phase-specific chemical identification, that limitation is stated explicitly rather than inferred beyond the available evidence.

RESULTS AND DISCUSSION

XRD Analysis and Spinel Structural Ordering

Neat chitosan exhibited a broad diffraction feature centred at approximately 2θ = 20.2°, consistent with its semi-crystalline hydrogen-bonded structure. The magnetic nanofiller displayed reflections at approximately 30.15°, 35.48°, 43.12°, 53.45°, 57.02°, and 62.61°, indexed as the (220), (311), (400), (422), (511), and (440) planes of a cubic spinel iron-oxide lattice [5, 7]. The peak positions overlap the reference patterns commonly assigned to magnetite (PDF/JCPDS 19-0629) and maghemite (PDF/JCPDS 39-1346); therefore, XRD establishes a spinel iron-oxide phase but does not by itself uniquely resolve the Fe_3O_4/γ-Fe_2O_3 core/shell distribution. The corresponding d-spacings calculated from the reported peak positions are listed in Table 1.

Table 1. Reported XRD reflections and calculated interplanar spacings for the spinel iron-oxide nanofiller.

2θ (°)	Plane (hkl)	d-spacing (nm)
30.15	(220)	0.2964
35.48	(311)	0.2530
43.12	(400)	0.2098
53.45	(422)	0.1714
57.02	(511)	0.1615
62.61	(440)	0.1484

Note: d-spacings were calculated from the reported 2θ values using Cu-Kα radiation (λ = 0.15418 nm).

The average apparent crystallite size obtained from the Scherrer equation was approximately 13.8 nm, and the calculated cubic lattice parameter was 0.8362 nm. This parameter lies between values typically associated with magnetite-rich and maghemite-rich spinel iron oxides and is consistent with partial oxidation of magnetite. In the composite films, the chitosan halo remained present while the relative contribution from spinel iron-oxide reflections increased with filler content. The absence of an explicitly reported α-Fe_2O_3 signature within the supplied peak list is also consistent with controlled oxidation that retained a spinel-type structure rather than complete conversion to hematite.

FT-IR Evidence for Chitosan/Iron–Oxide Interfacial Interaction

The FT-IR spectrum of neat chitosan contained a broad O–H/N–H stretching envelope near 3420 cm^{-1}, an amide-associated band around 1658 cm^{-1}, and an amino-group vibration near 1592 cm^{-1}. After incorporation of Fe_3O_4@γ-Fe_2O_3, the broad O–H/N–H band shifted to approximately 3385 cm^{-1} and the amino-related band shifted to approximately 1585 cm^{-1} with broadening. A strong feature near 582 cm^{-1} was assigned to Fe–O vibrations of the spinel iron-oxide phase. The principal assignments and shifts are summarized in Table 2.

Table 2. Diagnostic FT-IR bands of neat chitosan and the magnetic chitosan composite.

Neat chitosan (cm^{-1})	Composite (cm^{-1})	Assignment	Interpretation
3420	3385	O–H/N–H stretching	Shift to lower wavenumber; modified hydrogen-bonding environment.
1658	~1658	Amide-related vibration	Retained chitosan amide contribution.
1592	1585	–NH_2 bending / amino vibration	Shift and broadening consistent with interaction at amino sites.
—	582	Fe–O lattice vibration	Confirms incorporation of spinel iron oxide.

Note: FT-IR shifts support interfacial interaction but do not, on their own, prove a unique coordination geometry.

© STM Journals 2026. All Rights Reserved

The simultaneous changes in the O–H/N–H and amino regions support an altered local bonding environment at the chitosan/iron–oxide interface. The most defensible interpretation is a combination of hydrogen bonding and Lewis acid-base/coordination-type interaction between chitosan donor groups and surface iron sites [11, 12]. This interfacial coupling provides a plausible mechanism for improved stress transfer and reduced polymer-chain mobility in the composite, which is consistent with the mechanical and thermal trends discussed below.

HR-TEM Morphology and Core/Shell Dimensions

HR-TEM analysis showed approximately spherical nanoparticles with diameters in the range of 12–16 nm. The supplied contrast analysis described a darker inner region of approximately 9.5 nm and an outer oxidized region approximately 2.2 nm thick. Taking the shell thickness on both sides gives an overall diameter of approximately 13.9 nm, in close agreement with the 13.8 nm Scherrer crystallite size and within the reported HR-TEM size range [8]. A lattice fringe spacing of approximately 0.253 nm was observed and agrees with the calculated d-spacing for the (311) spinel plane (0.2530 nm; Table 1). Figure 2 summarizes the reported geometry without reproducing or simulating an experimental micrograph.

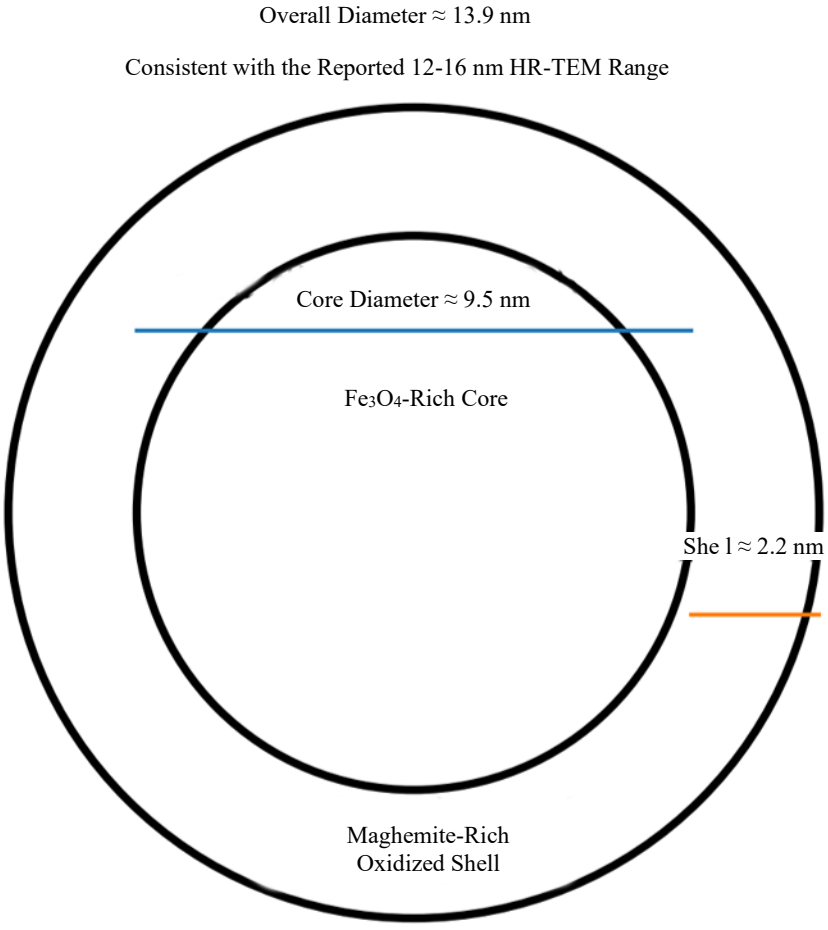


Figure 2. Schematic representation of the reported HR-TEM dimensions: An approximately 9.5 nm magnetite-rich inner region surrounded by an approximately 2.2 nm oxidized maghemite-rich surface region. This schematic is derived from the reported dimensions and is not a substitute for the original HR-TEM micrograph.

The dimensional agreement between XRD and HR-TEM suggests that the observed particles were largely single-crystalline or composed of only a small number of coherently diffracting domains.

© STM Journals 2026. All Rights Reserved

Nevertheless, the chemical identity of a 2.2 nm shell is difficult to establish solely from conventional TEM contrast because magnetite and maghemite have similar crystal structures. Phase-sensitive confirmation by X-ray photoelectron spectroscopy, Mössbauer spectroscopy, electron-energy-loss spectroscopy, or Raman spectroscopy would strengthen the core/shell assignment in future work.

Magnetic Properties at 300 K

The Fe_3O_4 precursor exhibited a reported saturation magnetization (M_s) of 68.2 emu g^{-1}, which decreased to 62.5 emu g^{-1} after controlled surface oxidation. The approximately 8.4% decrease is consistent with partial conversion of magnetite-rich material into a maghemite-rich oxidized phase and with enhanced surface spin disorder at nanoscale dimensions.

The oxidized nanoparticles retained only very small reported remanence (0.1 emu g^{-1}) and coercivity (2.1 Oe), compared with 1.2 emu g^{-1} and 12.5 Oe for the precursor. The reported magnetic properties are summarized in Table 3.

Table 3. Reported magnetic properties of the precursor, core/shell nanoparticles, and chitosan composites at 300 K.

Sample	M_s (emu g^{-1})	M_r (emu g^{-1})	Hc (Oe)
Fe_3O_4 precursor	68.2	1.2	12.5
Fe_3O_4@γ-Fe_2O_3	62.5	0.1	2.1
CS-1	12.4	0.0	0.0
CS-3	28.1	0.0	0.0
CS-5	42.8	0.0	0.0

Note: Composite M_s values are reproduced from the supplied dataset. Because magnetization scales with the mass used for normalization, the final experimental record should explicitly state whether composite values were normalized to total specimen mass or to magnetic-filler mass.

Within the supplied dataset, the reported magnetic response increased systematically from CS-1 to CS-5 (12.4, 28.1, and 42.8 emu g^{-1}, respectively), while remanence and coercivity were reported as effectively zero for the composite films. Figure 3 compares the reported M_s values.

The nearly closed room-temperature loops implied by negligible M_r and Hc are consistent with a highly reversible, superparamagnetic-like response at 300 K [7, 10]. A rigorous determination of superparamagnetic blocking behavior, however, requires temperature-dependent zero-field-cooled/field-cooled measurements and a clearly stated magnetization normalization basis.

Young's modulus increased from 1.15 GPa for CS-0 to 1.42, 1.85, and 2.38 GPa for CS-1, CS-3, and CS-5, representing approximate increases of 23.5%, 60.9%, and 107.0%, respectively (Figure 4). The simultaneous increase in strength and stiffness consists of efficient reinforcement by a rigid nanoscale phase and improved stress transfer across a chemically interacting polymer–particle interface.

The FT-IR band shifts provide independent qualitative support for this interpretation. The increasing trend also suggests that, within the tested 0–5 wt% range, any aggregation that occurred did not dominate the mechanical response sufficiently to reverse the reinforcement effect.

Mechanical Reinforcement

The tensile strength increased monotonically with magnetic-filler loading, from 32.4 MPa for neat chitosan to 38.2, 45.6, and 53.1 MPa for CS-1, CS-3, and CS-5, respectively. These values correspond to increases of approximately 17.9%, 40.7%, and 63.9% relative to neat chitosan. Figure 5 shows the loading dependence. The 5 wt% film, therefore, achieved an approximately 64% tensile-strength improvement within the composition range investigated.

© STM Journals 2026. All Rights Reserved

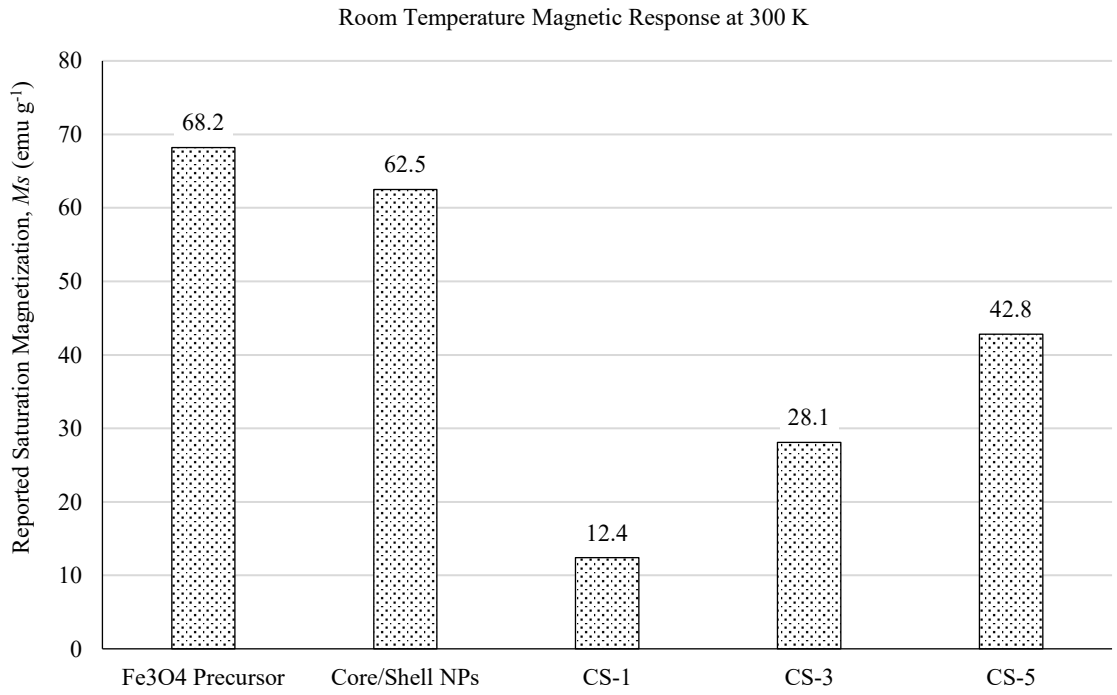


Figure 3. Reported saturation magnetization at 300 K for the Fe_3O_4 precursor, oxidized core/shell nanoparticles, and chitosan composites. Error bars are not shown because replicate-level magnetic data were not provided in the supplied dataset.

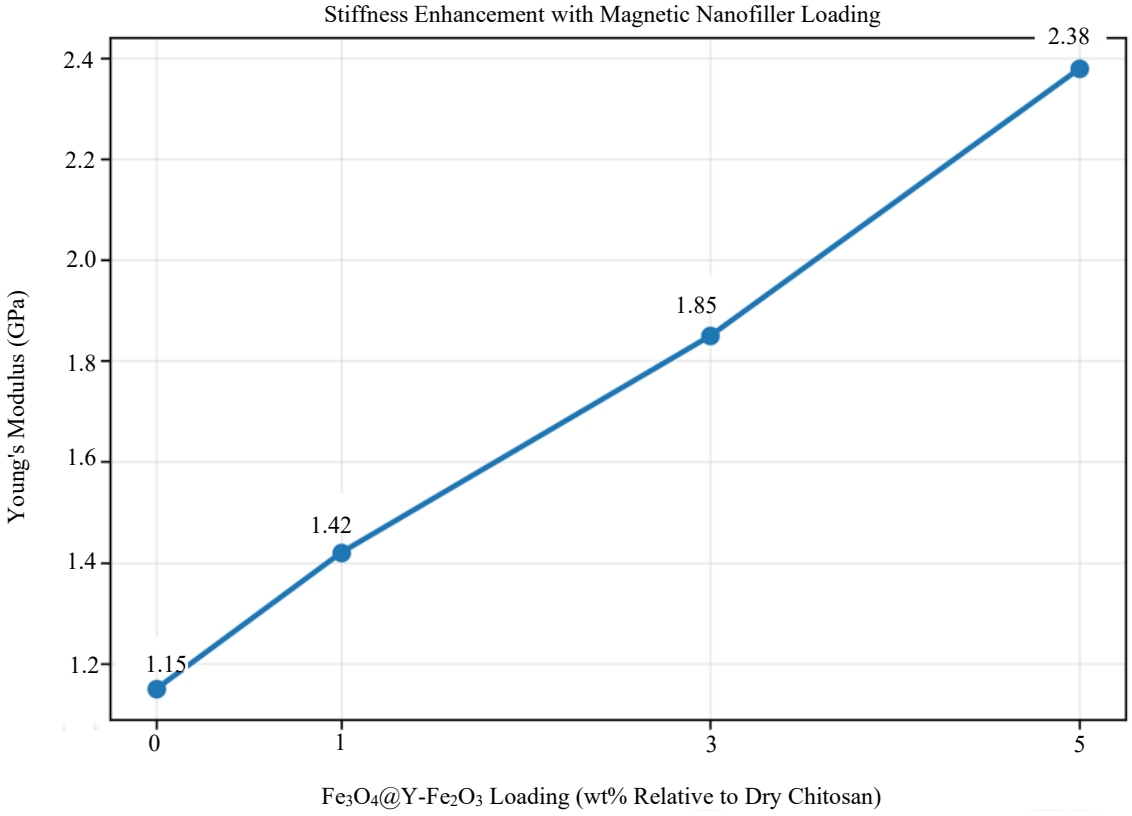


Figure 4. Young's modulus of neat chitosan and Fe_3O_4@γ-Fe_2O_3/chitosan films as a function of magnetic-filler loading.

© STM Journals 2026. All Rights Reserved

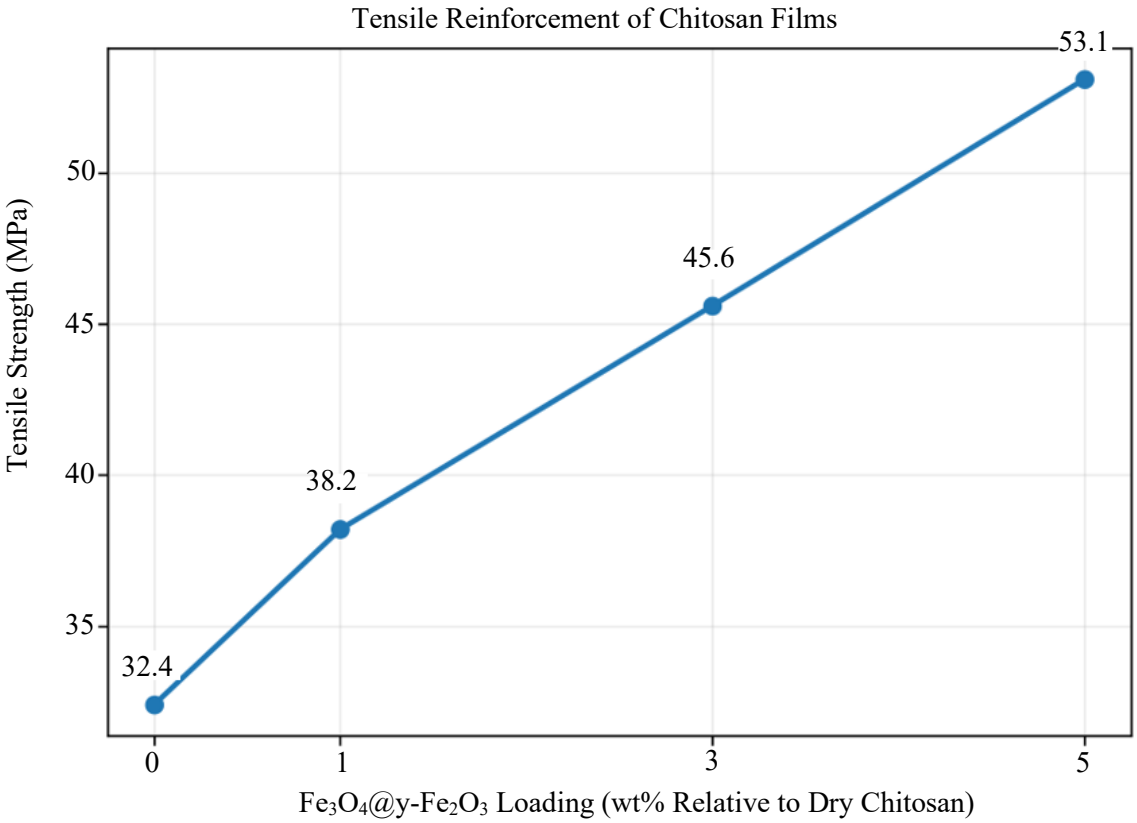


Figure 5. Tensile strength as a function of Fe_3O_4@γ-Fe_2O_3 loading in the chitosan films. Values are the reported central values supplied for the study.

Thermal Stability

TGA under nitrogen showed the expected multistage mass-loss behavior of chitosan-based materials. The low-temperature region (approximately 30–140°C) was associated primarily with loss of absorbed moisture. The principal polymer-degradation region occurred at approximately 220–380°C and was attributed to chitosan backbone decomposition and cleavage of glycosidic linkages, followed by higher-temperature decomposition of carbonaceous residues and remaining organic products. The reported degradation onset increased from 225°C for CS-0 to 233, 246, and 258°C for CS-1, CS-3, and CS-5, respectively (Figure 6).

The 33°C increase for CS-5 indicates that the inorganic phase and the polymer–particle interface hindered thermal motion and delayed the onset of rapid polymer degradation. The same interfacial immobilization mechanism invoked for mechanical reinforcement can, therefore, account for the thermal trend: strong local interactions reduce chain mobility, while the inorganic particles act as thermally stable barriers that alter the heat- and mass-transfer environment during decomposition.

Integrated Structure–Property Relationship

Taken together, the XRD, FT-IR, HR-TEM, mechanical, TGA, and magnetic results support a consistent structure–property picture. Nanoscale spinel iron oxide was retained after thermal oxidation, the reported particle dimensions were compatible across XRD and HR-TEM, and chitosan functional groups interacted measurably with the inorganic surface. As filler loading increased, the same interface that stabilized particle dispersion and transferred mechanical stress also restricted polymer-chain mobility, giving monotonic increases in tensile strength, modulus, and thermal-degradation onset. The magnetic phase simultaneously remained field-responsive after incorporation into the polymer matrix.

© STM Journals 2026. All Rights Reserved

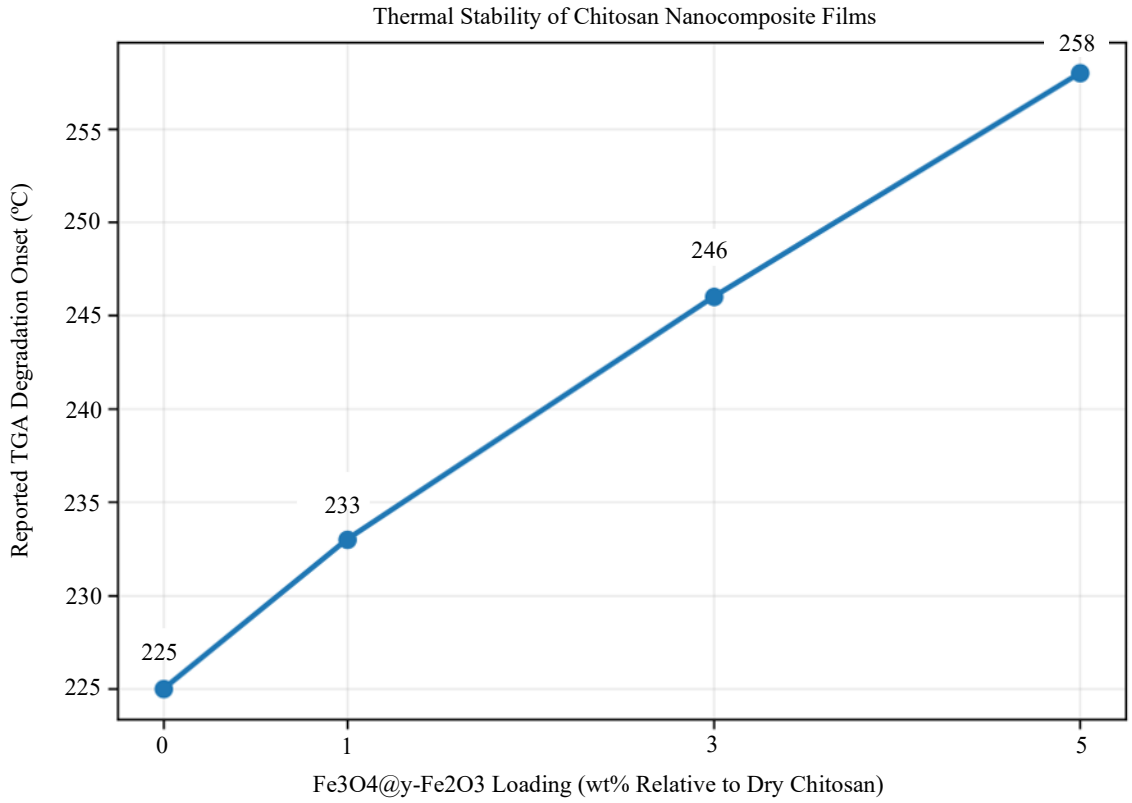


Figure 6. Reported TGA degradation-onset temperature as a function of Fe_3O_4@γ-Fe_2O_3 loading. The 5 wt% film shows a 33°C increase relative to neat chitosan.

Table 4. Selected magnetic, mechanical, and thermal properties of neat chitosan and Fe_3O_4@γ-Fe_2O_3/chitosan composite films.

Property	CS-0	CS-1	CS-3	CS-5
Magnetic filler (wt%)	0	1	3	5
M_s (emu g^{-1})	0.0	12.4	28.1	42.8
Tensile strength (MPa)	32.4	38.2	45.6	53.1
Young's modulus (GPa)	1.15	1.42	1.85	2.38
TGA onset (°C)	225	233	246	258

Note: Values are reproduced from the corrected supplied dataset. No standard deviations were available for the present descriptive comparison. The selected magnetic, mechanical, and thermal properties are summarized in Table 4.

The 5 wt% composition provided the strongest combined response among the tested formulations, but it should not be interpreted as a universal optimum because filler contents above 5 wt% were not investigated. At higher loadings, magnetic dipolar interactions and particle agglomeration could eventually reduce mechanical homogeneity or alter film flexibility. Optimization should, therefore, balance magnetic response against dispersion quality, toughness, water uptake, and application-specific transport properties.

Comparison with Previous Work and Application Perspective

The observed behavior is consistent with earlier reports showing that chitosan can stabilize or coat iron-oxide nanoparticles while retaining a useful magnetic response [13, 14, 21]. Soares et al. reported that chitosan/iron-oxide systems retain the characteristic thermal and magnetic properties of the magnetic phase [14], while Vaewbundit and Siriphannon demonstrated that chitosan/iron-oxide nanocomposites can be synthesized with useful magnetic characteristics [13]. More recent chitosan-

© STM Journals 2026. All Rights Reserved

coated superparamagnetic Fe_3O_4 systems have also emphasized the value of the chitosan interface for dispersion and functionalization [19]. The present work extends this theme to a thermally oxidized Fe_3O_4@γ-Fe_2O_3 nanofiller embedded at controlled low loadings in a cast chitosan film, with simultaneous evaluation of structural, interfacial, mechanical, thermal, and magnetic properties.

For near-term functional use, the most directly supported applications are magnetic separation, magnetic adsorbents, recoverable catalytic supports, and sensing or field-responsive films. Chitosan offers chemically active amino and hydroxyl groups for binding pollutants or biomolecules, while the magnetic phase can facilitate external-field handling. Biomedical applications – such as targeted drug delivery or hyperthermia – remain conceptually relevant to the material class [10, 15, 19], but the present dataset does not include cytocompatibility, sterility, particle-leaching, colloidal-stability, drug-loading, release, or alternating-field heating measurements; such claims, therefore, require dedicated validation before biomedical translation.

Study Limitations and Recommended Validation

Three limitations should be considered when interpreting the current dataset. First, conventional XRD cannot unambiguously distinguish magnetite from maghemite in nanoscale spinel mixtures because of strong peak overlap; phase-sensitive spectroscopy would strengthen the core/shell chemical assignment. Second, near-zero coercivity and remanence at one temperature are consistent with superparamagnetic-like behavior but do not define a blocking temperature; ZFC/FC magnetometry would provide that information. Third, the supplied dataset did not include raw instrument files, replicate-level uncertainties, or the explicit mass-normalization basis used for composite VSM values. Reporting these items in future datasets would improve reproducibility and enable formal statistical analysis.

CONCLUSIONS

Fe_3O_4@γ-Fe_2O_3-reinforced chitosan films were fabricated by co-precipitation, controlled thermal oxidation, and solution casting at 1–5 wt% magnetic-filler loading. XRD showed the characteristic cubic spinel pattern with an apparent crystallite size of approximately 13.8 nm and a lattice parameter of 0.8362 nm. HR-TEM indicated approximately spherical 12–16 nm particles, with a reported ~9.5 nm magnetite-rich inner region and ~2.2 nm oxidized outer region; the corresponding overall dimension (~13.9 nm) agreed closely with the XRD-derived size. FT-IR shifts in the O–H/N–H and amino-group regions, together with the Fe–O band near 582 cm^{-1}, supported interfacial interaction between chitosan and the iron-oxide surface.

At 300 K, the composite films exhibited negligible reported remanence and coercivity and a highly reversible magnetic response. Mechanical and thermal properties improved monotonically within the tested range: the 5 wt% film reached 53.1 MPa tensile strength, an approximately 64% increase over neat chitosan, while Young's modulus rose from 1.15 to 2.38 GPa and the reported TGA onset increased from 225 to 258°C. These trends are consistent with nanoparticle reinforcement, interfacial stress transfer, and restricted polymer-chain mobility. Among the investigated formulations, CS-5 provided the strongest combined magnetic, mechanical, and thermal response. The material is, therefore, a promising platform for magnetic separation, adsorption, sensing, and other field-responsive composite applications. Phase-specific shell verification, temperature-dependent magnetometry, explicit VSM mass normalization, and replicate-level statistical data would further strengthen future validation and application-specific translation.

REFERENCES

1. Laurent S, Forge D, Port M, Roch A, Robic C, Vander Elst L, et al. Magnetic iron oxide nanoparticles: Synthesis, stabilization, vectorization, physicochemical characterizations, and biological applications. Chem Rev. 2008;108(6):2064–2110.
2. Tartaj P, Morales MP, Veintemillas-Verdaguer S, González-Carreño T, Serna CJ. The preparation of magnetic nanoparticles for applications in biomedicine. J Phys D Appl Phys. 2003;36(13):R182–R197.

© STM Journals 2026. All Rights Reserved

3. Gupta AK, Gupta M. Synthesis and surface engineering of iron oxide nanoparticles for biomedical applications. Biomaterials. 2005;26(18):3995–4021.
4. Ali A, Zafar H, Zia M, Ul Haq I, Phull AR, Ali JS, et al. Synthesis, characterization, applications, and challenges of iron oxide nanoparticles. Nanotechnol Sci Appl. 2016;9:49–67.
5. Cornell RM, Schwertmann U. The Iron Oxides: Structure, Properties, Reactions, Occurrences and Uses. 2nd ed. Weinheim: Wiley-VCH; 2003.
6. Chikazumi S. Physics of Ferromagnetism. 2nd ed. Oxford: Clarendon Press; 1997.
7. Nguyen MD, Tran HV, Xu S, Lee TR. Fe_3O_4 nanoparticles: Structures, synthesis, magnetic properties, surface functionalization, and emerging applications. Appl Sci. 2021;11(23):11301.
8. Dave PN, Kalaniya RY. Synthesis and magnetic properties of Fe_3O_4@γ-Fe_2O_3 core/shell nanoparticles. J Indian Chem Soc. 2012;89(6):853–856.
9. Massart R. Preparation of aqueous magnetic liquids in alkaline and acidic media. IEEE Trans Magn. 1981;17(2):1247–1248.
10. Kim DK, Zhang Y, Voit W, Rao KV, Muhammed M. Synthesis and characterization of surfactant-coated superparamagnetic monodispersed iron oxide nanoparticles. J Magn Magn Mater. 2001;225(1–2):30–36.
11. Dash M, Chiellini F, Ottenbrite RM, Chiellini E. Chitosan - A versatile semi-synthetic polymer in biomedical applications. Prog Polym Sci. 2011;36(8):981–1012.
12. Bhattarai N, Gunn J, Zhang M. Chitosan-based hydrogels for controlled, localized drug delivery. Adv Drug Deliv Rev. 2010;62(1):83–99.
13. Vaewbundit S, Siriphannon P. Soft solution in situ synthesis of chitosan/iron oxide nanocomposites and their magnetic properties. Soft Matter. 2021;17(25):6238–6247.
14. Soares PIP, Machado D, Laia C, Pereira LCJ, Coutinho JT, Ferreira IMM, et al. Thermal and magnetic properties of chitosan-iron oxide nanoparticles. Carbohydr Polym. 2016;149:382–390.
15. Kadam AA, Lee DS. Glutaraldehyde cross-linked magnetic chitosan nanocomposites: Reduction precipitation synthesis, characterization, and application for removal of hazardous textile dyes. Bioresour Technol. 2015;193:563–567.
16. Pospiskova K, Safarik I. Low-cost, easy-to-prepare magnetic chitosan microparticles for enzymes immobilization. Carbohydr Polym. 2013;96(2):545–548.
17. Bae KH, Park M, Do MJ, Lee N, Ryu JH, Kim GW, et al. Chitosan oligosaccharide-stabilized ferrimagnetic iron oxide nanocubes for magnetically modulated cancer hyperthermia. ACS Nano. 2012;6(6):5266–5273.
18. Singh N, Riyajuddin S, Ghosh K, Mehta SK, Dan A. Chitosan-graphene oxide hydrogels with embedded magnetic iron oxide nanoparticles for dye removal. ACS Appl Nano Mater. 2019;2(11):7379–7392.
19. Mistral J, Ve Koon KT, Cotica LF, Dias GS, Santos IA, Alcouffe P, et al. Chitosan-coated superparamagnetic Fe_3O_4 nanoparticles for magnetic resonance imaging, magnetic hyperthermia, and drug delivery. ACS Appl Nano Mater. 2024;7(7):7097–7110.
20. Hall BD, Zanchet D, Ugarte D. Estimating nanoparticle size from diffraction measurements. J Appl Crystallogr. 2000;33(6):1335–1341.
21. Wu Y, Wang Y, Luo G, Dai Y. In situ preparation of magnetic Fe_3O_4-chitosan nanoparticles for lipase immobilization by cross-linking and oxidation in aqueous solution. Bioresour Technol. 2009;100(14):3459–3464.

© STM Journals 2026. All Rights Reserved